Assessment of Crystalline Materials for Solid State Lighting Applications: Beyond the Rare Earth Elements

Pier Carlo Ricci

Department of Physics, University of Cagliari, S.P. 8 Km 0.700, 09042 Monserrato, Cagliari, Italy; carlo.ricci@dsf.unica.it

check for updates

Abstract: In everyday life, we are continually exposed to different lighting systems, from the home interior to car lights and from public lighting to displays. The basic emission principles on which they are based range from the old incandescent lamps to the well-established compact fluorescent lamps (CFL) and to the more modern Light Emitting Diode (LEDs) that are dominating the actual market and also promise greater development in the coming years. In the LED technology, the key point is the electroluminescence material, but the fundamental role of proper phosphors is sometimes underestimated even when it is essential for an ideal color rendering. In this review, we analyze the main solid-state techniques for lighting applications, paying attention to the fundamental properties of phosphors to be successfully applied. Currently, the most widely used materials are based on rare-earth elements (REEs) whereas Ce:YAG represents the benchmark for white LEDs. However, there are several drawbacks to the REEs' supply chain and several concerns from an environmental point of view. We analyze these critical issues and review alternative materials that can overcome their use. New compounds with reduced or totally REE free, quantum dots, metal–organic framework, and organic phosphors will be examined with reference to the current state-of-the-art.

Keywords: solid state lightings; LED; phosphors; rare earths elements

1. Introduction

In recent years, light-emitting diode (LED) technology has reached high-quality standards and performance and competes with the traditional incandescent lamp as well as compact fluorescent lamps in terms of luminosity and ease of implementation. Moreover, LEDs present outstanding advantages over other lighting systems such as small size, high lifetime, high mechanical stability, and very high luminescence efficiency approaching the theoretical limits [1]. The latter is a mandatory target if we consider that approximately 20% of global energy consumption is due to lightning [2,3]. Hence, the requirements of energy-saving and the reduction of CO_2 emissions in the atmosphere have given an additional boost to the development of LEDs for lighting.

Given that light-emitting diodes produce quasi-monochromatic light, two main approaches have been pursued to obtain a white emission (WLED) (Figure 1): a combination of (at least) three LEDs, with power ratios adjusted to obtain white light with a specific color temperature (RGB (Red, Green, Blue)-LED); a single LED in combination with one or more phosphor material to partially or fully convert the LED emission (phosphor-converted LED). The two approaches are discussed below.

The first approach allows for the development of smart light sources, which can adapt their emission color intensity upon specific requests definable by the user. This approach permits the development of smart light sources, but has the great disadvantage related to the complexity and stability of the electronics. The spectral behavior of different LEDs strongly depends on the driving current and the chip temperature and should constantly be monitored. These drawbacks do not permit

the production and exploitation of RGB white LEDs for wide diffusion as well as in those applications where reliability and massive production are key parameters.

Figure 1. Schematic assembly to obtain white emission in light-emitting diode (LED) technology.

In contrast to the RGB approach, a single LED light source can be combined with one or more phosphor materials to obtain white light.

Two strategies can be further distinguished. The first uses a blue LED and converts part of the emitted light to longer wavelengths by means of phosphor material; the obtained white color is from the combination of the residual blue and the down-converted emission. In the second, the white perceived light arises from the fully converted emission from a (near) ultraviolet LED through different phosphors with an overall large emission in the visible spectrum. The latter approach is not widely used because of the higher costs of UV LED pumping and the intrinsic losses of efficiency during the conversion process, but it permits a wider choice in the possible phosphor materials and to achieve improved lighting performances.

Currently, most of the commercially available LED-based white light sources rely on a visible emission (generally in 400–450 nm spectral range) and partially converted emissions in the remaining visible spectral range from phosphors. Up to now, most of the WLEDs are based on the combination of a blue LED (GaN-based) and a YAG matrix ($Y_3Al_5O_{12}$) doped with cerium as emitter centers. The ubiquity of Ce:YAG phosphors and hence, the single phosphor configuration, in commercial devices is related to the very simple and cost-effective fabrication as well as the long-term stability of the phosphor, related to the high melting point and stable thermal and chemical properties.

The alternatives proposed to tune the emission concern new matrices, new luminescent dopants, or the combination of two or more dopant elements, but most of these solutions still utilize rare-earth ions for their superior efficiency as phosphors and their high chemical stability.

The emission of rare-earth ions is generally due to optical transitions within the f-manifold [4]. The f-electrons are well shielded from the chemical environment and therefore almost retain their atomic character. As a consequence, the f–f emission spectra consist of sharp lines. These radiative recombinations are generally slow (microseconds to milliseconds) due to the recombination selection rule (partially forbidden or totally spin forbidden). On the other hand, when the recombination is related to 5d–4f optical transitions, the emission band is relatively broad (such as Eu^{2+} ($^4f_7$) and, mainly, for LED application, Ce^{3+} ($^4f_1$), the d–f optical transitions are allowed and consequently, the recombination is much faster (tens of ns in the case of Ce^{3+}, depending on the matrix).

Aside from the historical reasons, the term "rare" for these elements is still justified today, not only for their effective "rare" condition, but mostly for their high supply disruption risk and the environmental issues related to their mining and refinement [5]. Rare earth production is concentrated in a few geographical regions and mining extraction has a strong environmental impact. For this reason, valid alternatives to REEs in photoelectronic devices with particular regard to lighting systems are strongly required.

In this review, we analyzed the requirements for good white emission in LEDs and the parameters useful for a definitive assessment. A brief review of candidates for next-generation light emitters in

substitution of In–Ga-based LEDs is also presented. Furthermore, advances in phosphors for LED application, with particular attention on the materials that substitute or strongly reduce the use of the rare-earth elements, is reported.

2. Session 1: The Electroluminescent Pumping Devices

Light-emitting diodes (LEDs) are usually made of single- or multi-layer semiconductors containing the p–n junction, where under the electric bias condition, electrons and holes flow from the electrodes to the junction region or the semiconductor layer to combine and emit incoherent light. The wavelength of the emitted light is determined by the energy bandgap of the semiconductor material. This mechanism is at the base of the large and increasing use of LED systems in lighting devices and the 2014 Nobel Prize was awarded for the development of blue LED with high efficiency and a long lifetime. In direct bandgap semiconductors like gallium nitride, most of the excited electrons in the conduction band recombine with holes in the valence band without any change in momentum from a phonon. The energy versus momentum plots show that for an electron to recombine in an indirect semiconductor (e.g., silicon, GaP), additional momentum is required in the form of a phonon, paying the involvement of the phonon with reduced optical efficiency. For these reasons, indirect semiconductors are poorly used for LEDs. Another key point in the choice of the electroluminescent material is the possibility of easily creating a p–n homojunction or to obtain a heterojunction in combination with other compounds. Moreover, the stability of the compounds should be guaranteed with an easily reproducible degree and, finally, have low cost. Last but not least, there is a need for a suitable substrate with a lattice parameter similar to the electroluminescent compound.

The conjunction of all these parameters has strongly encouraged the development of InGaN based white LED where the emission wavelength varies from deep blue (375 nm) to blue (up to 450 nm) by changing the content of indium in the GaN matrix. Suitable and efficient alternatives are still in the R&D phase, but show great limitations in efficiency or stability:

Zinc oxide is attracting extraordinary attention due to its promising properties such as a wide direct band gap of 3.3 eV and a very high exciton binding energy of 60 meV [6]. These properties make ZnO light-emitting diodes potentially useful in efficient solid-state lighting alternatives to GaN-based LEDs. However, only a few electroluminescent devices have been fabricated successfully with low stability [7,8].

The relatively low mobility of ZnO compared to GaN and nearly four times stronger electron–phonon coupling, together with relatively low thermal conductivity, are serious shortcomings for ZnO. The real challenge with ZnO is the realization of the homojunction, particularly, the p-type ZnO is difficult to obtain in a well reproducible and low-cost way [9]. On the other hand, heterojunctions have been realized using various p-type materials such as Si [10], GaN [11], AlGaN [12], $SrCu_2O_2$ [13], NiO [14], ZnTe [15], Cu_2O [16], SiC [17], $ZnRh_2O_4$ [18], and GaAs [19–21]. However, the stability issue remains the main reason that has hampered the development of these devices.

Other alternatives are represented by II–VI compounds, and in particular, to ZnSe [22]. The emission covers from the blueish to near UV to green, and it possesses a direct bandgap, however, the difficulty of reaching a heavily doped sample with good reproducibility has led to relatively low efficiency and short life.

SiC-based LED devices have already been commercialized [23]; however, it is an indirect bandgap material, and, again, it is difficult to obtain high brightness.

As reported in the table below (Table 1), the semiconductors utilized in the LED light-emitting layer were based on gallium. Therefore, at the moment, there are no alternatives at the high technology readiness level available that are free of such elements.

Table 1. Electroluminescent peak emission of selected semiconductors.

Semiconductor Material	Emission Wavelength (nm)
GaAs	850–940
GaAsP	630–660
GaAsP	605–620
GaAsP:N	585–595
AlGaP	550–570
SiC	430–505
GaInN	430–460

Recently, a real breakthrough has been reported in solid-state lighting emitting devices, represented by the use of metal halide perovskites [24]. Green, red, and near-infrared perovskites-based LEDs have achieved high external quantum efficiencies and relatively stable working conditions. Such structures have the general structural formula ABX3, where A is a cation such as a methylammonium (MA), formamidinium (FA) or Cs^+; B is a metal (typically Pb^{2+} or Sn^{2+}); and X is a halogen (I, Br). Recently, total inorganic perovskites have also been developed, $CsPbX_3$ (X = I, Br), showing increased properties compared to organic–inorganic halide perovskites (e.g., $MAPbBr_3$ and $FAPbBr_3$), and for their higher photoluminescence quantum efficiency and thermal stability [25,26].

Degradation by heat, moisture, and light are the main issues to be solved in organic/inorganic perovskites, while an intrinsic structural instability hampers the development of fully inorganic perovskites. Indeed, $CsPbX_3$ perovskites crystallize in four different structures: cubic phase (α), tetragonal phase (β), orthorhombic phase (γ), and orthorhombic phase (δ). However, only in the α phase is it possible to develop an efficient device. On the other hand, at room temperature, α-CsPbI3 is not thermodynamically stable and great efforts are being finalized to define the best strategies to develop a stable phase under ambient conditions.

MoO_3-ammonia treated PEDOT:PSS (poly(3,4-ethylenedioxythiophene) polystyrene sulfonate) was used in all-inorganic $CsPbBr_3$ perovskite LEDs to obtain efficient and stable emission (on the order of a couple of hours of continuous operations), while in [26], the stabilization of the α-CsPbI3 phase was achieved by in situ formations of perovskite nanocrystals (NCs), obtaining 1200 min operation time and shelf stability of over two months, which is much longer than the actual hybrid perovskite-based LED. The hybridization of the structure was further utilized by using polymer nanofiber as the protective layer, where a polymer matrix (polymethylmethacrylate, PMMA) incorporated the $CsPbBr_3$ quantum dots, improving the stability and maintaining excellent optical properties [27]. The embedding of the perovskites in transparent matrices like SiO_2 and Al_2O_3 [28,29]) has been developed and obtained good stability (in the order of tens of days).

However, different issues need to be explored in this field such as efficiency, mass production, toxicity, and mainly, the operational stability (at least continuous working conditions) should be solved before real commercialization. An overview of the state-of-the-art of inorganic lead perovskites and the relative device engineering can be found in [30].

3. Session 2: Properties of the Phosphor

The first step consists of a focused overview of the requirements of phosphors for LED application with particular regard on the performance of Ce:YAG [31]:

Emission spectrum: The emission spectrum of the phosphor is strictly connected to the pumping LED. If the pumping LED lies in the near UV spectral range, the phosphor should cover all the visible region. On the other hand, when a visible LED is chosen, the emission of the phosphor will be mixed with the partially transmitted light of the pumping LED. In this case, the peak emission wavelength of the LED light source is generally chosen at about 450 nm, whereas the pumping energy and the eye sensitivity are still high. The peak emission wavelength of the phosphors should be between 500 and 600 nm in case of only one kind of phosphor, while in the case of multiple phosphors, they typically

cover up to 700 nm, partially overlapping each other. Ce:YAG has a very broad emission spectrum with a full width at half maximum (FWHM)of typically 100 nm due to the spin-orbit split ground state of Ce^{3+}. Its yellow emission (centered at about 560 nm), in combination with part of the blue emission from the pumping LED, yields a "white light" and the color rendering is moderate (about 70).

At this point, some words are needed to better define the parameters of a white source, and in particular, to determine its suitability for lighting applications. Good emission efficiency of the radiation within the human sensitivity and high color quality of the light are fundamental requests. The first is defined by the luminous efficiency of the radiation (LER) as the brightness of the radiation averaged by human eye response [32]:

$$LER\left(\frac{lm}{W}\right) = 683 \frac{\int_{360}^{830} I(\lambda)V(\lambda)d\lambda}{\int_{360}^{830} I(\lambda)d\lambda} \tag{1}$$

where $I(\lambda)$ is the emission spectrum and $V(\lambda)$ is the eye sensitivity curve. The highest value obtained was 683 lm/W from monochromatic radiation at 555 nm where the eye sensitivity peak occurred. Thus, since the white emission has a contribution at both lower and higher wavelengths (blue and red components, respectively), the LER is always less than 683 lm/W, generally about 350 lm/W.

The CIE coordinates are often utilized to define the color of a broad emission, while for a lighting source suitable for lighting application, different parameters need to be considered. Since the effects depend on the absorption and reflectivity spectra, the response of an object to optical radiation is different from source to source, and also, if both can be optically perceived as "white". The widely accepted parameters that define the response after illumination is the color rendering index (CRI) [33]. The CRI is calculated by comparing the color of test objects when illuminated by the light source, with the colors of the objects obtained by illuminating a reference source (generally a calibrated incandescent lamp). The correlated color temperature (CCT) of a light source is obtained by comparing its emission spectrum with the black body curve that better matches the emitted light.

The CRI can even be calculated as a function of the distance of the reflected coordinates of at least eight standard colors [33]:

$$CRI = 100 - 4.6 \frac{1}{8} \sum_{1}^{8} \Delta E_i \tag{2}$$

where ΔE_i is the distance between the colors of test object I, illuminated with the test and reference source. This value was close to 100, and the response of the test source to the incandescent test lamp was closer.

Excitation spectrum: The second important criterion is the spectral excitability of the phosphors, (i.e., as already stated, the matching between the excitation spectrum and the emission of the pumping LEDs). Hence, phosphors with good excitability in the near-UV to the blue region of the spectrum are required. In general, the increase of the temperature close to the junction of the LED can alter the optical properties of the materials, and a relatively wide excitation spectrum is preferred to compensate such variations. On the other hand, it remains that the overlap between the absorption of the phosphors and the emission should be avoided to minimize the auto-absorption process.

Ce:YAG can be excited by the blue pumping LED with a sufficiently broad excitation band near 450 nm showing good overlap with the LED's emission spectrum (GaN-based). The spin-allowed parity-allowed 4f–5d absorption leads to high absorption strength and the high limit before concentration quenching permits up to 5 wt % of cerium ions in the YAG matrix to be reached [34].

Thermal behavior: Since the phosphor is situated close to the LED chip, the thermal dependence of the optical properties is of great importance. Indeed, only approximately 10–20% of the input electrical power is converted to optical power while the remaining power produces heat to be dissipated by the device. Even in LED devices, a small percentage of the electrical power is dissipated in thermal energy (about 20%), and temperatures from 400 K up to 450 K can be reached close to the small area of the chip. As a consequence, it is required that the phosphor maintain its optical properties at these temperatures. Indeed, shifting and/or broadening of the emission spectrum can alter the

emission color of the entire device as well as generate a decrease in quantum efficiency. Furthermore, at this temperature, the excitation spectrum can also change, thus influencing the absorbed fraction of the emission of the pumping LED, further contributing to variation in the light perceived. In this framework, Ce:YAG has excellent thermal quenching behavior, maintaining more than 50% of the room temperature emission intensity at 700 K [34] and with slight modification (thermal broadening) of the emission spectrum.

Quantum efficiency (Q.Y.): The internal Q.Y. is defined as the ratio between the number of emitted photons and the number of absorbed photons, while the external Q.Y. represents the ratio between the number of emitted photons and the number of incident photons. Both parameters are fundamental in the choice of suitable phosphors and they should be as close as possible to 1.

In general, increasing the dopant concentration in a phosphor material increases the absorption at the excitation wavelength. However, there exists a trade-off between the increasing absorption (and emission) and a decrease in the internal quantum efficiency due to concentration quenching [35]. If the internal Q.Y. is a characteristic of the materials and its relationship with incoming light, the external Q.Y. also depends on the structure and morphology of the LED devices. For instance, in the case of a phosphor layer of low dimensioned particles, scattering of the converted light will lead to increased absorption losses, thus lowering the total number of photons extracted from the phosphor layer [36]. Scattering losses depend on the particle size and their spatial and size distribution, with broad particle size distribution typically leading to uneven emission colors. From this aspect, the achievement of nanosized Ce:YAG particles with high Q.Y. is still a challenge [37].

Long term stability: The lifetime of a LED is defined as the time it takes until its light output, or lumen maintenance, reaches 70% of the initial output. This is also called L70.

Current commercially available products mention lifetimes typically from 15,000 to 100,000 h. The high lifetime with respect to the old lighting devices such as incandescent lamps or CFL is mostly connected to the electrical part and to the design. The heat dissipation is the biggest issue, and as a consequence, the quality of the component is of fundamental importance. However, even the phosphors should guarantee similar performance across a long period, and in this sense, chemical and photostability are the main issues (i.e., several stability problems have been reported for sulfide-based phosphors (such as CaS:Eu and SrS:Eu) due to the low stability in air [38,39]). Ce:YAG shows a high thermal stability that is also preserved under high photon fluence.

Saturation: This is defined as a sub-linear dependence of the light emitted with respect to the excitation intensity. This parameter is strongly connected to the temporal behavior of the radiative decay path and hence to the time decays' constant of the emitted light. This parameter is most important when a high flux of excitation photons interact with the phosphor, where it is necessary that the absorption and the re-emitted light remain an efficient process. In this view, relative fast decay time (ns time range) is preferred. Concerning Ce:YAG, due to the allowed nature of the emission transition in Ce^{3+}, the decay constant remains well below 100 ns in YAG [40], and even faster in different matrices [40–43].

4. Session 3: Rare-Earth-Based Phosphors

Some of the above-mentioned six requirements are primarily related to the properties of the dopant ions such as the shape of the emission band, while others are influenced by the composition of the host material such as the chemical and thermal stability. Several other requirements are related to the interplay between host and dopant such as thermal quenching behavior. The main drawback of Ce:YAG lies in the lack of emission above 600 nm, decreasing the color rendering and the CCT. To reduce this effect, different strategies have been exploited: adding further luminescent ions or tune the crystal field, by varying the element in the matrix. Both should be considered carefully. For example, Eu^{3+} gives a very efficient red emission, but it is not excited at 450 nm, like most of the REEs in the YAG matrix. One strategy already exploited utilizes other rare-earth elements as a sensitizer for new emissions. It has already been proven that there is a waterfall effect between cerium

to terbium to europium: the excited d levels of Ce^{3+} have an efficient energy transfer to $^5D_3$ levels of Tb^{3+} that, after internal relaxation to $^5D_4$, pass the energy to the $^5D_{0,1}$ levels of europium [44–47]. Obviously, the efficiency of such processes as well as the final emission strongly depends on the relative concentration among the different dopants.

Another option to tune the emission is related to the variation of the crystalline field close to the emitting ions by compositional tuning of mixed garnet materials. In the case of shielded-electrons of trivalent rare-earth ions, the perturbations can be treated in the weak-field approximation where the strength of the crystal field is smaller than the Coulomb interaction of the electrons with each other and the spin-orbit coupling interaction [48]. The shift of the PL bands can be interpreted by a variation of the crystalline field due to modifications of the reticular parameters associated with the presence of different elements in the A and B position of the general $A_3B_5O_{12}$ (A = Y and B = Al in YAG). Some examples are related to the substitution of Al by Ga or Sc as well as the substitution of Y with Gd [49,50]. Substitution of Al^{3+} by a combination of Mg^{2+} and Si^{4+} leads to a considerable shift of the emission maximum to 600 nm, allowing the fabrication of a warm-white LED with relatively high color rendering [51].

Other possibilities to improve color rendering properties consist of the combination of different phosphors such as $SrGa_2S_4:Eu^{2+}$ (green phosphor) mixed with a red-emitting material ($Ca_{1-x}Sr_xS:Eu^{2+}$ [52,53], $Sr_2Si_5N_8:Eu^{2+}$ [54] or $Sr[Li_2Al_2O_2N_2]:Eu^{2+}$ [55]) or directly mixing the red phosphor ($K_2SiF_6:Mn^{4+}$) in combination with Ce:YAG [56]. Finally, high CRI was obtained by the three-doped YAG matrix (Ce, Mn, Pr) [57] and by using Ce:YAG, $Sr[LiAl_3N_4]:Eu^{2+}$ double phosphors [58] (84 and 90, respectively).

In this respect, the number of red-emitting phosphors adequate for high-luminance applications is rather small and europium is the most applied dopant as $(Ba,Sr)_2Si_5N_8:Eu$ [59] or $(Ca,Sr)SiAlN_3:Eu$ (emission between 610–660 nm, Ref [60]). However, the rather broad emission bands from Eu^{2+} greatly limit the maximum achievable luminous efficiency of warm-white LEDs because a significant emission spectrum is obtained where the sensitivity range of the human eye is lower. Materials with narrower emission such as the sulfide material ($Sr_{1-x}Ca_xS:Eu$) exhibit attractive luminescence properties [61], but strong emission quenching with temperature, hydrophobicity, hydrolysis, and, mostly, the toxicity of the hydrolysis products (H_2S gas) hinders commercial application. Recently, a new red phosphor with high efficiency was proposed, $Sr(LiAl_3N_4):Eu^{2+}$, which is excitable by GaN-based blue LEDs and has low thermal quenching [58].

On the other hand, alternative nitride phosphors require extreme and expensive preparation conditions including high temperature and high nitrogen pressures. Moreover, these phosphors commonly exhibit fluorescence reabsorption and non-uniformity of luminescent properties, resulting in the loss of luminous efficiency and time-dependent shift of color point [62,63].

The near UV excitation gave impressive results from a CRI point of view, reaching a value close to the unity in the $BaMgAl_{10}O_{17}:Eu^{2+}$, $Ca_9La(PO_4)_7:Eu^{2+},Mn^{2+}$ double phosphors, Eu^{2+}, Dy^{3+}, Ce^{3+}/Tb^{3+}, β-$Na_2Ca_4(PO_4)_2(SiO_4)$, and in Ce^{3+}-doped $Ca_2YHf_2Al_3O_{12}$ [64–66].

As has already been pointed out, the highest and incoming inconvenience related to all these phosphors that can really limit the diffusion of LED lighting systems is the massive presence of rare-earth elements (in Ce:YAG in particular).

5. Session 4: Criticisms of Rare-Earth

Rare-earth elements have been recently inserted in the critical raw materials list, not for their effective "rare" condition, but mostly because of their high supply disruption risk.

The first criticality analysis for raw materials was published in 2010 by an Ad-Hoc Working Group on Defining Critical Raw Materials. Fourteen critical raw materials were identified from a candidate list of 41 non-energy, non-food materials. In 2011, the EU Commission formally adopted this list and stated that it would continue to monitor the issue of critical raw materials to identify priority actions. The list was further updated in 2014 and 2017, reaching 27 key elements in the last version [67] (see Table 2).

Table 2. Critical Raw Materials List defined by the EU Commission in 2017.

2017 Critical Raw Materials List			
Antimony	Fluorspar	LREEs	Phsphorus
Baryte	Gallium	Magnesium	Scandium
Beryllium	Germanium	Natural graphite	Silicon metal
Bismuth	Hafnium	Natural rubber	Tantalum
Borate	Helium	Niobium	Tungsten
Cobalt	HREEs	PGMs	Vanadium
Coking coal	Indium	Phosphate rock	-

Abbreviations: HREEs, heavy rare-earth elements; LREEs, light rare-earth elements; and PGMs for platinum group metals.

Although global REE reserves are widely distributed, the current production of REEs is highly localized in a few geographical zones. The EU considers three factors when assessing the criticality of a mineral: (i) the economic importance of the mineral; (ii) its supply risk; and (iii) its environmental country risk (i.e., the potential that environmental regulations could restrict access to the mineral deposits). On these bases, the table below was built.

One of the most critical factors for rare-earth elements is that of the time requirement for new mines: REE selection, extraction, processing, and purification are extremely energy and water-intensive. Moreover, the time needed for real production is much longer than that of other minerals (e.g., gold), where the shortest pre-production period for a mine can be two years or less, while REE mines take seven to fifteen years to bring REE mines into the production phase. The processing of RE elements is a complex process that involves multiple steps and refining. Solvent extraction, flotation processes, and electrolytic processes are often needed to separate the rare-earth from other metals. Moreover, all REE deposits contain some level of uranium and thorium, and the deposit can easily be over the threshold radioactive threshold.

Some other processes are still needed to separate the selected rare-earth element. Cracking of the mineral, separation, and reduction of the rare-earth oxide are utilized to obtain the final rare-earth alloy (or oxide) [68]. It is worth pointing out that the steps require a large amount of water, energy, and chemicals with a high environmental impact. As an example, the Chinese government committed 4 billion Yuan ($600 million) in 2012 to clean up the damage caused by the RE sector in the region close to the city of Baotou [69].

The recycling of rare-earth elements is still limited and is limited to a definite sector (magnet). The total recycling of REEs is no more than a few percent, however, some avenues have begun to be explored [70,71]. From an ecological point of view and toward the possibility of solving the supply disruption, the recycling process could be the definitive solution, however, the cost of REE extraction from the final products makes recovery uncompetitive from an economical point of view. End-products contain small amounts of metals targeted for recycling (g to mg) and the incorporation of target metals makes the separation of recyclable material difficult and expensive.

In 2020, it is foreseen that about 375,000 tons of rare-earth elements are stocked (300,000 only in magnet applications), where the recycled amount in 2020 has been counted to be between 5000 and 10,000 tons, highlighting the needed to increase this sector [70].

## 6. Session 5: Beyond Rare-Earth Elements in White LED

The aim of a large part of the actual research (which is also commercially driven and looking to the future) is to develop a new white phosphor-converted LED where REEs are no longer present (nor as phosphor as an element of the matrix) by overcoming the color and/or temperature breakdowns of Ce:YAG containing current WLEDs, but preserving or even increasing the high performances in fulfilling the six key requirements listed above.

Different approaches are being exploited to reach this result, particularly by developing a white converted LED with the help of quantum dot semiconductor nanoparticles or by exploiting the potentialities of pure organic and organic–inorganic hybrid compounds.

To achieve a tailored spectrum in white light, semiconductor nanocrystals, known as quantum dots, may provide a reliable alternative. Quantum dots (QD) behave like phosphors, but their emission can be tuned among the visible spectrum by changing the physical size of the dot. For lighting applications of the quantum dots (QLED), a white emission from QDs is required.

The QLED performance is highly dependent on the choice of charge injection materials (electron and hole transport layer, HTL and ETL, respectively) where they should possess high carrier mobility as well as balance the electron/hole injections (Figure 2). According to the type of electron transport layers, the structure of QLEDs can be distinguished as an organic/QD bilayer, all-organic electron transport layer, all-inorganic electron transport layer, and organic/inorganic electron transport layer.
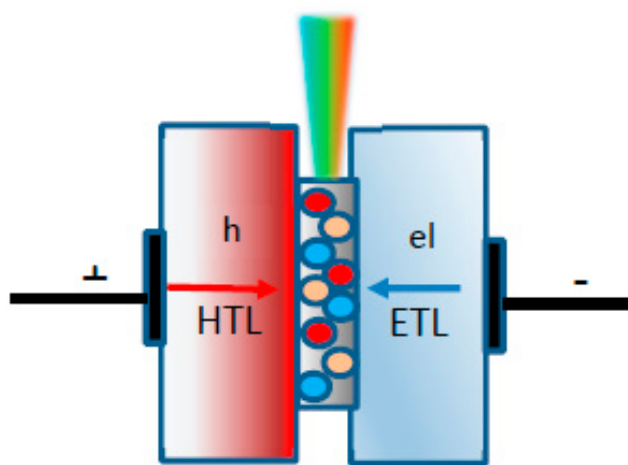
Figure 2. Schematic representation of QLED white emission.

The key role is obviously represented by the QD. Cadmium sulfide and, mostly, cadmium selenide have been widely studied and have already been successfully applied in displays and potentially for white LED applications [72,73]. They present a relatively high quantum yield (>80%) but, mostly, they present a wide tunability as a function of the dimension of the dots. [74]. The relative narrow emission (in the order of tens of nanometer) associated with the possibility to be pumped by a blue LED increases their possibility of being applied in display technology (such as Q-LED TV). The working principle of QDs in displays depends on two basic strategies, very similar to that for LED technology, which is the use of three different QDs to achieve the RGB strategy or to use a white QD emission and suitable color filters (CFs).

Current color filter technology acts as a passive optical component that, coupled with the selective transmission of light through any combination of sub-pixels (via LCD), results in full RGB colors.

Quantum dot core-shell heterostructures give further degrees of freedom in the development of highly efficient phosphors. CdSe/CdS/ZnS and CdSe/ZnS/CdSZnS colloidal nanoparticles were successfully utilized to obtain blue-pumped white emission with a Q.Y. of 0.85 and 85 lm/W and 105 lm/W for green, blue-based white light generation [75].

On the other hand, the presence of Cd strongly discourages the application in white LED, where the massive use of the devices as well as the difficulty in the recycling process can have a strong impact on the environmental aspect. A second technological aspect that needs to be considered is the thermal quenching aspect, which strongly suggests the remote approach in the design of the LED.

In order to go beyond this issue, other materials have been studied. InP is the most promising material since it possesses similar optical and electronic properties to cadmium based quantum dots [73,76].

However, the performance of both the optical properties (efficiency, color quality) and stability are far from that of Cd-QD. A wider overview of QD materials and devices can be found in [77].

An interesting emerging solution is represented by carbon-based quantum dots. Carbon dots (C-dots) have similar optical properties to semiconductor quantum dots. The advantage is represented by much lower cost in production and mainly in the environmental impact, and these issues have generated great interest in the scientific community. C-dots can be obtained with several different precursors and methods, but at the moment, the reproducibility and stability of C-dot based devices are not advanced enough for real commercial production.

Citric acid (CA) was successfully applied as a precursor for C-dots [78] that permits easy surface passivation and, hence, increased stability. Other strategies have been to embed them in a silica matrix or to dope with B, N, S, Si, and P organics to improve their quantum yield and increase the stability [79,80].

Despite the large interest in C-dots, there is still a lack of comprehension of the exact mechanism of their luminescence: a nanosized carbon core, surface states, the formation of molecular species, and resonance cross-linked enhanced effect are the main theories about the possible emission mechanism.

Organic luminescence converters have been investigated as attractive alternatives because of their broad absorption and emission, moderate price, and ease of fabrication. There have been several attempts to use organic luminescence converters for LED applications, but up till now, there has been great concern for their stability (thermal and in critical environmental) and their integration with the actual devices.

One of the most studied and promising organic materials are carbon nitride-based compounds [81]. Of most interest is the thermal and structural stability (up to 550 °C) as well as the simple and low-cost synthesis procedure. Graphitic carbon nitride (g-C_3N_4) can be obtained by direct condensation of nitrogen-containing organic precursors (e.g., urea, thiourea, dicyandiamide, cyanamide, and guanidine hydrochloride) [82–84]. The possibility of tuning the optical properties of carbon nitride was exploited by doping with specific elements (among the others Fe, Ag, Br, P, Br, I) [83,85,86] or by slightly changing the long-range order of the organic framework [87,88]. In this view, doping with the phenyl group gives rise to an internal Q.Y. up to 60% (excited at 440 nm) and a broad emission over the visible spectrum with a CRI of 0.88. The stability of a prototype was tested for over 9000 h [89].

The two basic reasons that hindered the use of organic phosphors in solid-state lighting is given as the requirement to work in a solution to decrease the formation of aggregation effects (formation of a dimer, in general) and to avoid thermal quenching. One strategy consists of utilizing the remote phosphors design and to insert the organic compound into a proper external polymetric matrix [90,91]. The effect partially solves the mentioned issues, assuring a proper separation among the emitting units and hindering the formation of aggregates as well as preserving low-temperature, thanks to the increased distance from the p–n junction. Another option is to protect the organic core with an external mesh (inorganic) to increase the stability against the environmental conditions and the photogeneration of surface groups [92,93]. On the other hand, the concentration quenching effect hampers a large amount of organic compound and the resistance at high luminous flux can decrease the stability of the devices.

Metal–organic frameworks (MOFs), or coordination polymers, are a class of regular crystalline solids with well-organized host structures formed by metal cations coordinated with organic units [94]. Although MOFs are widely studied for different applications ranging from catalysis [95,96], non-linear optics [97], and magnetism [98], they present a high potential for luminescent devices given the possibility of incorporating a light-emitting cluster directly in the organic/metal mesh, allowing the modulation of luminescent properties [99,100]. The luminescence can be obtained as a metal-centered emission or luminescent absorbates, related to the organic liker through a ligand localized emission or metal-to-ligand charge transfer. Mostly, the metal ions are represented by a rare-earth for ease in the integration process, however, alternatives have already been developed. Some examples are represented by zinc-based MOFs, where a full RGB was obtained in a single structure, iridium complex,

and organic dyes encapsulated in a MOF [101]. The high porosity of MOFs can be utilized to insert guest molecules within their frameworks. In this last strategy, it is possible to insert dyes with a different optical emission, so the final emitted color of the composite can be easily modulated by simply adjusting the amount and component of dyes [102,103]. Furthermore, a mesoporous blue-emitting MOF was prepared as a host to encapsulate a yellow emitting iridium complex, and the final device presented a good color temperature (5409 K) and high quantum yield up to 115 °C [104].

7. Conclusions and Perspectives

In this paper, we discussed the main requirements and materials in solid-state lighting devices.

Considering that the emissions from a LED are intrinsically monochromatic or, better defined by the semiconductor gap, we analyzed the fundamental techniques for obtaining a white emission. The choice to use three LEDs (RGB) creates an excellent possibility to tune and control the color emitted, but it is not handy for real use in widely diffused lighting systems. The most utilized structure involves the use of a single LED, whose emission was totally (near UV emission) or partially (emission between 400 and 450 nm) used to excite one or more phosphors. The photoconverted emission spectrum covered the entire visible spectrum, creating the desired with relative simplicity.

The choice of materials useful for the excitation process (LED) is quite narrow. The most widely used structure is the InGaN and by varying the percentage between In and Ga, the electroluminescence can be varied between 375 and 450 nm. Most of the alternatives are represented by gallium based materials; while ZnO shows great potential, the difficulty of obtaining stable p–n junctions inhibits the creation of stable devices.

A real breakthrough has been reported in solid-state lighting emitting devices, represented by the use of metal halide perovskites, although their stability is far from being long enough for a real commercial application, however, currently, perovskites represent an intriguing option with high potentiality at lab scale.

It is necessary to pay great attention to the choice of the phosphor and it is generally based on the requirements discussed in this review: emission spectrum, excitation spectrum, thermal stability, internal and external quantum efficiency, long term stability, and saturation effects have been indicated and discussed as key issues. Among the different phosphors, Ce:YAG represents the real benchmark to be overcome. The ubiquity of Ce:YAG phosphors in commercial devices is related to their very simple and cost-effective fabrication as well as their long-term stability. The excitation spectrum overlaps the emission of the InGaN LED at 450 nm, while the broad emission covers the visible spectrum, but with a low CRI. Alternatives utilized in commercial devices are mostly contained to other rare-earth-based phosphors, and the presence of only a few alternatives free of lanthanides underline the disruption supply and the environmental problems connected to this class of element.

Quantum dots could represent a reliable option, but environmental issues (cadmium based) and long-term stability (carbon dots) need to be solved.

Although they have the lowest thermal stability of most organic phosphors, carbon nitride-based materials present a structural stability up to 500 °C and its optical properties satisfy the general requirements of phosphors and high potential of development.

Finally, coordination polymers or MOF give broad tunability options, and if the long-term stability is solved they could represent an intriguing option to be applied in lighting devices.

The research in phosphors and materials for lighting devices is still open and continues to represent a forefront field of development. Review of the actual results is mandatory to help future research, even if the large efforts of researchers in this field do not permit a summary in a single publication of a fully comprehensive report.

Conflicts of Interest: The author declares no conflict of interest.

References

1. Cangeloso, S. *LED Lighting: A Primer to Lighting the Future*; O'Reilly Media, Inc.: Sebastopol, CA, USA, 2012; ISBN 9781449334765.

2. Humphreys, C.J. Solid-State Lighting. *MRS Bull.* **2008**, *33*, 459–470. [CrossRef]

3. Zissis, G. Energy Consumption and Environmental and Economic Impact of Lighting: The Current Situation. In *Handbook of Advanced Lighting Technology*; Springer Science and Business Media LLC: Berlin, Germany, 2016; pp. 1–13.

4. Withnall, R.; Silver, J. Physics of Light Emission from Rare-Earth Doped Phosphors. In *Handbook of Visual Display Technology*; Springer Science and Business Media LLC: Berlin, Germany, 2012; pp. 1019–1028.

5. Ganguli, R.; Cook, U.R. Rare earths: A review of the landscape. *MRS Energy Sustain.* **2018**, *5*, 5. [CrossRef]

6. Janotti, A.; Van De Walle, C.G. Fundamentals of zinc oxide as a semiconductor. *Rep. Prog. Phys.* **2009**, *72*, 126501. [CrossRef]

7. Lima, S.; Cremona, M.; Davolos, M.R.; Legnani, C.; Quirino, W. Electroluminescence of zinc oxide thin-films prepared via polymeric precursor and via sol–gel methods. *Thin Solid Films* **2007**, *516*, 165–169. [CrossRef]

8. Rahman, F. Zinc oxide light-emitting diodes: A review. *Opt. Eng.* **2019**, *58*, 010901. [CrossRef]

9. Fan, J.; Sreekanth, K.; Xie, Z.; Chang, S.; Rao, K.V. p-Type ZnO materials: Theory, growth, properties and devices. *Prog. Mater. Sci.* **2013**, *58*, 874–985. [CrossRef]

10. Baltakesmez, A.; Tekmen, S.; Köç, P.; Tüzemen, S.; Meral, K.; Onganer, Y. UV-visible detector and LED based n-ZnO/p-Si heterojunction formed by electrodeposition. *AIP Adv.* **2013**, *3*, 032125. [CrossRef]

11. Yang, L.; Wang, Y.; Xu, H.; Liu, W.; Zhang, C.; Wang, C.; Wang, Z.; Ma, J.; Liu, Y. Color-Tunable ZnO/GaN Heterojunction LEDs Achieved by Coupling with Ag Nanowire Surface Plasmons. *ACS Appl. Mater. Interfaces* **2018**, *10*, 15812–15819. [CrossRef]

12. Ding, M.; Guo, Z.; Zhou, L.; Fang, X.; Zhang, L.; Zeng, L.; Xie, L.; Zhao, H. One-Dimensional Zinc Oxide Nanomaterials for Application in High-Performance Advanced Optoelectronic Devices. *Crystals* **2018**, *8*, 223. [CrossRef]

13. Ohta, H.; Orita, M.; Hirano, M.; Hosono, H. Fabrication and characterization of ultraviolet-emitting diodes composed of transparent p-n heterojunction, p-SrCu$_2$O$_2$ and n-ZnO. *J. Appl. Phys.* **2001**, *89*, 5720–5725. [CrossRef]

14. Deng, R.; Yao, B.; Li, Y.; Xu, Y.; Li, J.; Li, B.; Zhang, Z.; Zhang, L.; Zhao, H.; Shen, D. Ultraviolet electroluminescence from n-ZnO/p-NiO heterojunction light-emitting diode. *J. Lumin.* **2013**, *134*, 240–243. [CrossRef]

15. Schrier, J.; Demchenko, D.O.; Wang, L.-W.; Alivisatos, A.P.; Wang, L.-Y.; Alivisatos, A.P. Optical Properties of ZnO/ZnS and ZnO/ZnTe Heterostructures for Photovoltaic Applications. *Nano Lett.* **2007**, *7*, 2377–2382. [CrossRef] [PubMed]

16. Ievskaya, Y.; Hoye, R.L.Z.; Sadhanala, A.; Musselman, K.; MacManus-Driscoll, J. Fabrication of ZnO/Cu$_2$O heterojunctions in atmospheric conditions: Improved interface quality and solar cell performance. *Sol. Energy Mater. Sol. Cells* **2015**, *135*, 43–48. [CrossRef]

17. Shi, Z.; Wang, J.; Zhang, B.; Du, G.; Xia, X.; Yin, W.; Zhang, S.; Wang, H.; Zhao, L.; Dong, X. Dominant ultraviolet electroluminescence from p-ZnO:As/n-SiC(6H) heterojunction light-emitting diodes. *Appl. Phys. Lett.* **2012**, *100*, 101112. [CrossRef]

18. Ohta, H.; Mizoguchi, H.; Hirano, M.; Narushima, S.; Kamiya, T.; Hosono, H. Fabrication and characterization of heteroepitaxial p-n junction diode composed of wide-gap oxide semiconductors p-ZnRh$_2$O$_4$/n-ZnO. *Appl. Phys. Lett.* **2003**, *82*, 823–825. [CrossRef]

19. Zhang, X.; Wu, D.; Geng, H. Heterojunctions Based on II-VI Compound Semiconductor One-Dimensional Nanostructures and Their Optoelectronic Applications. *Crystals* **2017**, *7*, 307. [CrossRef]

20. Gao, Z.; Lu, L.; Xue, X.; Li, J.; Zhao, L.; Ahmad, D.; Li, H. Comparative Study of ZnO Nanostructures Grown on Variously Orientated GaN and AlxGa1−xN: The Role of Polarization, and Surface Pits. *Crystals* **2019**, *9*, 663. [CrossRef]

21. Borysiewicz, M.A. ZnO as a Functional Material, a Review. *Crystals* **2019**, *9*, 505. [CrossRef]

22. Katayama, K.; Matsubara, H.; Nakanishi, F.; Nakamura, T.; Doi, H.; Saegusa, A.; Mitsui, T.; Matsuoka, T.; Irikura, M.; Takebe, T.; et al. ZnSe-based white LEDs. *J. Cryst. Growth* **2000**, *214*, 1064–1070. [CrossRef]

23. Fuchs, F.; Soltamov, V.A.; Väth, S.; Baranov, P.G.; Mokhov, E.N.; Astakhov, G.V.; Dyakonov, V. Silicon carbide light-emitting diode as a prospective room temperature source for single photons. *Sci. Rep.* **2013**, *3*, 1637. [CrossRef]

24. Lin, K.; Xing, J.; Na Quan, L.; De Arquer, F.P.G.; Gong, X.; Lu, J.; Xie, L.; Zhao, W.; Zhang, D.; Yan, C.; et al. Perovskite light-emitting diodes with external quantum efficiency exceeding 20 per cent. *Nature* **2018**, *562*, 245–248. [CrossRef] [PubMed]

25. Liu, K.-K.; Liu, Q.; Yang, D.-W.; Liang, Y.-C.; Sui, L.-Z.; Wei, J.-Y.; Xue, G.-W.; Zhao, W.-B.; Wu, X.-Y.; Dong, L.; et al. Water-induced MAPbBr$_3$@PbBr(OH) with enhanced luminescence and stability. *Light Sci. Appl.* **2020**, *9*, 44. [CrossRef] [PubMed]

26. Luo, D.; Chen, Q.; Qiu, Y.; Zhang, M.; Liu, B. Device Engineering for All-Inorganic Perovskite Light-Emitting Diodes. *Nanomaterials* **2019**, *9*, 1007. [CrossRef] [PubMed]

27. Chen, L.-C.; Tien, C.-H.; Tseng, Z.-L.; Dong, Y.-S.; Yang, S. Influence of PMMA on All-Inorganic Halide Perovskite CsPbBr$_3$ Quantum Dots Combined with Polymer Matrix. *Materials* **2019**, *12*, 985. [CrossRef] [PubMed]

28. Huang, S.; Li, Z.; Kong, L.; Zhu, N.; Shan, A.; Li, L. Enhancing the Stability of CH$_3$NH$_3$PbBr$_3$ Quantum Dots by Embedding in Silica Spheres Derived from Tetramethyl Orthosilicate in "Waterless" Toluene. *J. Am. Chem. Soc.* **2016**, *138*, 5749–5752. [CrossRef] [PubMed]

29. Kim, A.; Lee, H.; Kwon, H.-C.; Jung, H.S.; Park, N.-G.; Jeong, S.; Moon, J. Fully solution-processed transparent electrodes based on silver nanowire composites for perovskite solar cells. *Nanoscale* **2016**, *8*, 6308–6316. [CrossRef]

30. Cheng, G.; Liu, Y.; Chen, T.; Chen, W.; Fang, Z.; Zhang, J.; Ding, L.; Li, X.; Shi, T.; Xiao, Z. Efficient All-Inorganic Perovskite Light-Emitting Diodes with Improved Operation Stability. *ACS Appl. Mater. Interfaces* **2020**, *12*, 18084–18090. [CrossRef]

31. Smet, P.F.; Parmentier, A.B.; Poelman, D. Selecting Conversion Phosphors for White Light-Emitting Diodes. *J. Electrochem. Soc.* **2011**, *158*, R37. [CrossRef]

32. Choudhury, A.K.R. *Principles of Colour and Appearance Measurement*; Elsevier: Amsterdam, The Netherlands, 2014; Volume 2, ISBN 9781782423881.

33. Guo, X.; Houser, K. A review of colour rendering indices and their application to commercial light sources. *Light Res. Technol.* **2004**, *36*, 183–197. [CrossRef]

34. Lisitsyn, V.; Tulegenova, A.; Polisadova, E.; Lipatov, E.; Vaganov, V.; Lisitsyna, L.; Ju, Y. Nanodefects in YAG:Ce-Based Phosphor Microcrystals. *Crystals* **2019**, *9*, 476. [CrossRef]

35. Ricci, P.C.; Salis, M.; Corpino, R.; Carbonaro, C.M.; Fortin, E.; Anedda, A. A kinetics model for Tb^{3+} recombinations in low doped Tb: Lu$_{1.8}$Y$_{0.2}$SiO$_5$ crystals. *J. Appl. Phys.* **2010**, *108*, 043512. [CrossRef]

36. Li, J.; Tang, Y.; Tang, Y.; Ding, X.; Yuan, D.; Yu, B. Study on Scattering and Absorption Properties of Quantum-Dot-Converted Elements for Light-Emitting Diodes Using Finite-Difference Time-Domain Method. *Materials* **2017**, *10*, 1264. [CrossRef] [PubMed]

37. Armetta, F.; Saladino, M.L.; Giordano, C.; Defilippi, C.; Marciniak, L.; Hreniak, D.; Caponetti, E. Non-conventional Ce:YAG nanostructures via urea complexes. *Sci. Rep.* **2019**, *9*, 3368. [CrossRef] [PubMed]

38. Gang, S.-R.; Kim, D.; Kim, S.-M.; Hwang, N.; Lee, K.-C. Improvement in the moisture stability of CaS:Eu phosphor applied in light-emitting diodes by titania surface coating. *Microelectron. Reliab.* **2012**, *52*, 2174–2179. [CrossRef]

39. Xia, Q.; Batentschuk, M.; Osvet, A.; Winnacker, A.; Schneider, J. Quantum yield of Eu^{2+} emission in (Ca$_{1-x}$Sr$_x$)S:Eu light emitting diode converter at 20–420 K. *Radiat. Meas.* **2010**, *45*, 350–352. [CrossRef]

40. Lempicki, A.; Berman, E.; Wojtowicz, A.; Balcerzyk, M.; Boatner, L.A. Cerium-doped orthophosphates: New promising scintillators. *IEEE Trans. Nucl. Sci.* **1993**, *40*, 384–387. [CrossRef]

41. Rooh, G.; Kim, H.J.; Park, H.; Kim, S.; Jiang, H. Cerium-Doped Cs$_2$NaGdCl$_6$Cs$_2$NaGdCl$_6$ Scintillator for X-Ray and γ-Ray Detection. *IEEE Trans. Nucl. Sci.* **2013**, *61*, 397–401. [CrossRef]

42. Ricci, P.C.; Carbonaro, C.M.; Casu, A.; Cannas, C.; Corpino, R.; Stagi, L.; Anedda, A. Optical and structural characterization of cerium doped LYSO sol–gel polycrystal films: Potential application as scintillator panel for X-ray imaging. *J. Mater. Chem.* **2011**, *21*, 7771. [CrossRef]

43. Baccaro, S.; Blaẑek, K.; De Notaristefani, F.; Maly, P.; Mares, J.; Pani, R.; Pellegrini, R.; Soluri, A. Scintillation properties of YAP:Ce. *Nucl. Instrum. Methods Phys. Res. Sect. A Accel. Spectrom. Detect. Assoc. Equip.* **1995**, *361*, 209–215. [CrossRef]

44. Chiriu, D.; Stagi, L.; Ricci, P.C.; Corpino, R.; Ricci, P.C. Energy transfer mechanism between Ce and Tb ions in sol–gel synthesized YSO crystals. *Mater. Chem. Phys.* **2016**, *171*, 201–207. [CrossRef]

45. Thomas, K.; Alexander, D.; Sisira, S.; Gopi, S.; Biju, P.; Unnikrishnan, N.V.; Joseph, C. Energy transfer driven tunable emission of Tb/Eu co-doped lanthanum molybdate nanophosphors. *Opt. Mater.* **2018**, *80*, 37–46. [CrossRef]

46. Chiriu, D.; Stagi, L.; Carbonaro, C.; Corpino, R.; Casula, M.; Ricci, P.C. Towards the development of new phosphors with reduced content of rare earth elements: Structural and optical characterization of Ce:Tb: Al_2SiO_5. *Mater. Res. Bull.* **2016**, *77*, 15–22. [CrossRef]

47. Silveira, W.S.; Nascimento, P.A.; Silva, A.J.; Rezende, M.V.S. Luminescent properties and energy transfer mechanism from Tb^{3+} to Eu^{3+} doped in $Y_3Al_5O_{12}$ phosphors. *J. Alloys Compd.* **2020**, *822*, 153651. [CrossRef]

48. Wojtowicz, A. Physics of Solid-State Laser Materials. *Acta Phys. Pol. A* **1991**, *80*, 193–205. [CrossRef]

49. Tucureanu, V.; Matei, A.; Mihalache, I.; Danila, M.; Popescu, M.C.; Bita, B. Synthesis and characterization of YAG:Ce,Gd and YAG:Ce,Gd/PMMA nanocomposites for optoelectronic applications. *J. Mater. Sci.* **2014**, *50*, 1883–1890. [CrossRef]

50. Anedda, A.; Carbonaro, C.; Chiriu, D.; Ricci, P.C.; Aburish-Hmidat, M.; Guerini, M.; Lorrai, P.; Fortin, E. Compositional Tuning of Photoluminescence Properties in Nd-Doped YAG–YSGG Mixed Structures. *IEEE J. Quantum Electron.* **2006**, *42*, 563–569. [CrossRef]

51. Shang, M.; Fan, J.; Lian, H.; Zhang, Y.; Geng, D.; Lin, J. A Double Substitution of Mg^{2+}–Si^{4+}/Ge^{4+} for $Al(1)^{3+}$–$Al(2)^{3+}$ in Ce^{3+}-Doped Garnet Phosphor for White LEDs. *Inorg. Chem.* **2014**, *53*, 7748–7755. [CrossRef]

52. Xia, Q.; Batentschuk, M.; Osvet, A.; Richter, P.R.; Häder, D.-P.; Schneider, J.; Wondraczek, L.; Winnacker, A.; Brabec, C.J. Red-emitting $Ca_{1-x}Sr_xS:Eu^{2+}$ Phosphors as Light Converters for Plant-growth Applications. In Proceedings of the Materials Research Society Symposium, Boston, MA, USA, 28 November–2 December 2011; Cambridge University Press (CUP): Cambridge, UK, 2011; Volume 1342, pp. 67–72.

53. Cho, Y.-S.; Huh, Y.-D. Cathodoluminescence Properties of Red-Emitting $Sr_{1-x}Ca_xS:Eu$ Phosphors. *Bull. Korean Chem. Soc.* **2016**, *37*, 991–996. [CrossRef]

54. Piao, X.; Horikawa, T.; Hanzawa, H.; Machida, K.-I. Characterization and luminescence properties of $Sr_2Si_5N_8:Eu^{2+}$ phosphor for white light-emitting-diode illumination. *Appl. Phys. Lett.* **2006**, *88*, 161908. [CrossRef]

55. Hoerder, G.J.; Seibald, M.; Baumann, D.; Schröder, T.; Peschke, S.; Schmid, P.C.; Tyborski, T.; Pust, P.; Stoll, I.; Bergler, M.; et al. Sr[Li2Al2O2N2]:Eu^{2+}-A high performance red phosphor to brighten the future. *Nat. Commun.* **2019**, *10*, 1824. [CrossRef]

56. Sijbom, H.F.; Verstraete, R.; Joos, J.J.; Poelman, D.; Smet, P.F. $K_2SiF_6:Mn^{4+}$ as a red phosphor for displays and warm-white LEDs: A review of properties and perspectives. *Opt. Mater. Express* **2017**, *7*, 3332. [CrossRef]

57. Ma, Y.; Zhang, L.; Zhou, T.; Sun, B.; Wang, Y.; Kang, J.; Gao, P.; Huang, J.; Selim, F.A.; Wong, C.-P.; et al. High recorded color rendering index in single Ce,(Pr,Mn):YAG transparent ceramics for high-power white LEDs/LDs. *J. Mater. Chem. C* **2020**, *8*, 4329–4337. [CrossRef]

58. Pust, P.; Weiler, V.; Hecht, C.; Tücks, A.; Wochnik, A.S.; Henß, A.-K.; Wiechert, D.; Scheu, C.; Schmidt, P.J.; Schnick, W. Narrow-band red-emitting Sr[LiAl3N4]:Eu^{2+} as a next-generation LED-phosphor material. *Nat. Mater.* **2014**, *13*, 891–896. [CrossRef]

59. Lee, B.; Lee, S.; Jeong, H.G.; Sohn, K.-S. Solid-State Combinatorial Screening of $(Sr,Ca,Ba,Mg)_2Si_5N_8:Eu^{2+}$ Phosphors. *ACS Comb. Sci.* **2011**, *13*, 154–158. [CrossRef] [PubMed]

60. Chen, L.; Lin, C.-C.; Yeh, C.-W.; Liu, R.-S. Light Converting Inorganic Phosphors for White Light-Emitting Diodes. *Materials* **2010**, *3*, 2172–2195. [CrossRef]

61. Lakshmanan, A. *Luminescence and Display Phosphors: Phenomena and Applications*; Nova Publishers: Hauppauge, NY, USA, 2008; ISBN 9781614701972.

62. Leano, J.L., Jr.; Fang, M.-H.; Liu, R.-S. Critical Review—Narrow-Band Emission of Nitride Phosphors for Light-Emitting Diodes: Perspectives and Opportunities. *ECS J. Solid State Sci. Technol.* **2017**, *7*, R3111–R3133. [CrossRef]

63. Xie, R.-J.; Hirosaki, N.; Li, Y.; Takeda, T. Rare-Earth Activated Nitride Phosphors: Synthesis, Luminescence and Applications. *Materials* **2010**, *3*, 3777–3793. [CrossRef]

64. Huang, C.-H.; Chen, T.-M. $Ca_9La(PO_4)_7:Eu^{2+},Mn^{2+}$: An emission-tunable phosphor through efficient energy transfer for white light-emitting diodes. *Opt. Express* **2010**, *18*, 5089–5099. [CrossRef]

65. Li, K.; Shang, M.; Geng, D.; Lian, H.; Zhang, Y.; Fan, J.; Lin, J. Synthesis, Luminescence, and Energy-Transfer Properties of β-$Na_2Ca_4(PO_4)_2(SiO_4)$:A (A = Eu^{2+}, Dy^{3+}, Ce^{3+}/Tb^{3+}) Phosphors. *Inorg. Chem.* **2014**, *53*, 6743–6751. [CrossRef]

66. Liang, J.; Devakumar, B.; Sun, L.; Wang, S.; Sun, Q.; Huang, X.; Balaji, D. Full-visible-spectrum lighting enabled by an excellent cyan-emitting garnet phosphor. *J. Mater. Chem. C* **2020**, *8*, 4934–4943. [CrossRef]

67. Dewulf, J.; De Matos, C.T.; Baranzelli, C.; Ciupagea, C.; Dias, P.; Kayam, Y.; Pavel, C.; Peiròn, L.T.; Tzimas, E.; Vidal-legaz, B.; et al. Methodology for establishing the EU list of Critical Raw Materials. *Publ. Off. Eur. Union* **2017**, 1–25. [CrossRef]

68. Filho, W.L. An Analysis of the Environmental Impacts of the Exploitation of Rare Earth Metals. In *Rare Earths Industry*; Elsevier BV: Amsterdam, The Netherlands, 2016; pp. 269–277.

69. Ali, S. Social and Environmental Impact of the Rare Earth Industries. *Resources* **2014**, *3*, 123–134. [CrossRef]

70. Jowitt, S.M.; Werner, T.T.; Weng, Z.; Mudd, G.M. Recycling of the rare earth elements. *Curr. Opin. Green Sustain. Chem.* **2018**, *13*, 1–7. [CrossRef]

71. Ricci, P.C.; Murgia, M.; Ricci, P.C.; Sgariotto, S.; Stagi, L.; Corpino, R.; Chiriu, D.; Grilli, M.L. New life of recycled rare earth-oxides powders for lighting applications. In *IOP Conference Series: Materials Science and Engineering*; IOP Publishing: Bristol, UK, 2018; Volume 329, p. 012002.

72. Bae, W.K.; Lim, J.; Lee, N.; Park, M.; Lee, H.; Kwak, J.; Char, K.; Lee, C.; Lee, S. R/G/B/Natural White Light Thin Colloidal Quantum Dot-Based Light-Emitting Devices. *Adv. Mater.* **2014**, *26*, 6387–6393. [CrossRef]

73. Lee, K.-H.; Han, C.-Y.; Kang, H.-D.; Ko, H.; Lee, C.; Lee, J.; Myoung, N.; Yim, S.-Y.; Yang, H. Highly Efficient, Color-Reproducible Full-Color Electroluminescent Devices Based on Red/Green/Blue Quantum Dot-Mixed Multilayer. *ACS Nano* **2015**, *9*, 10941–10949. [CrossRef] [PubMed]

74. Zhang, H.; Su, Q.; Chen, S. Recent progress in the device architecture of white quantum-dot light-emitting diodes. *J. Inf. Disp.* **2019**, *20*, 169–180. [CrossRef]

75. Sadeghi, S.; Kumar, B.G.; Melikov, R.; Aria, M.M.; Jalali, H.B.; Nizamoglu, S. Quantum dot white LEDs with high luminous efficiency. *Optics* **2018**, *5*, 793–802. [CrossRef]

76. Kim, H.; Lee, W.; Moon, H.; Kim, S.J.; Chung, H.K.; Chae, H. Interlayer doping with p-type dopant for charge balance in indium phosphide (InP)-based quantum dot light-emitting diodes. *Opt. Express* **2019**, *27*, A1287–A1296. [CrossRef]

77. Lim, J.; Park, M.; Bae, W.K.; Lee, N.; Lee, S.; Lee, C.; Char, K. Highly Efficient Cadmium-Free Quantum Dot Light-Emitting Diodes Enabled by the Direct Formation of Excitons within InP@ZnSeS Quantum Dots. *ACS Nano* **2013**, *7*, 9019–9026. [CrossRef]

78. Mura, S.; Ludmerczki, R.; Stagi, L.; Garroni, S.; Carbonaro, C.M.; Ricci, P.C.; Casula, M.F.; Malfatti, L.; Innocenzi, P. Integrating sol-gel and carbon dots chemistry for the fabrication of fluorescent hybrid organic-inorganic films. *Sci. Rep.* **2020**, *10*, 1–12. [CrossRef]

79. Carbonaro, C.M.; Chiriu, D.; Stagi, L.; Casula, M.F.; Thakkar, S.V.; Malfatti, L.; Suzuki, K.; Ricci, P.C.; Corpino, R. Carbon Dots in Water and Mesoporous Matrix: Chasing the Origin of their Photoluminescence. *J. Phys. Chem. C* **2018**, *122*, 25638–25650. [CrossRef]

80. Zholobak, N.; Popov, A.; Shcherbakov, A.B.; Popova, N.R.; Guzyk, M.M.; Антонович, B.; Yegorova, A.V.; Scrypynets, Y.V.; Leonenko, I.; Baranchikov, A.; et al. Facile fabrication of luminescent organic dots by thermolysis of citric acid in urea melt, and their use for cell staining and polyelectrolyte microcapsule labelling. *Beilstein J. Nanotechnol.* **2016**, *7*, 1905–1917. [CrossRef] [PubMed]

81. Guo, Q.; Wei, M.; Zheng, Z.; Huang, X.; Song, X.; Qiu, S.; Yang, X.; Liu, X.; Qiu, J.; Dong, G. Full-Color Chemically Modulated g-C$_3$N$_4$ for White-Light-Emitting Device. *Adv. Opt. Mater.* **2019**, *7*, 1–11. [CrossRef]

82. Bledowski, M.; Wang, L.; Ramakrishnan, A.; Khavryuchenko, O.V.; Khavryuchenko, V.D.; Ricci, P.C.; Strunk, J.; Cremer, T.; Kolbeck, C.; Beranek, R. Visible-light photocurrent response of TiO$_2$–polyheptazine hybrids: Evidence for interfacial charge-transfer absorption. *Phys. Chem. Chem. Phys.* **2011**, *13*, 21511–21519. [CrossRef] [PubMed]

83. Feng, Y.; Liao, C.-Z.; Kong, L.; Wu, D.; Liu, Y.; Lee, P.-H.; Shih, K. Facile synthesis of highly reactive and stable Fe-doped g-C$_3$N$_4$ composites for peroxymonosulfate activation: A novel nonradical oxidation process. *J. Hazard. Mater.* **2018**, *354*, 63–71. [CrossRef]

84. Sun, J.; Phatake, R.; Azoulay, A.; Peng, G.; Han, C.; Barrio, J.; Xu, J.; Wang, X.; Shalom, M. Covalent Functionalization of Carbon Nitride Frameworks through Cross-Coupling Reactions. *Chem. A Eur. J.* **2018**, *24*, 14921–14927. [CrossRef]

85. Thorat, N.; Yadav, A.; Yadav, M.; Gupta, S.; Varma, R.; Pillai, S.; Fernandes, R.; Patel, M.; Patel, N. Ag loaded B-doped-g C$_3$N$_4$ nanosheet with efficient properties for photocatalysis. *J. Environ. Manag.* **2019**, *247*, 57–66. [CrossRef]

86. Wang, X.; Chen, X.; Thomas, A.; Fu, X.; Antonietti, M. Metal-Containing Carbon Nitride Compounds: A New Functional Organic-Metal Hybrid Material. *Adv. Mater.* **2009**, *21*, 1609–1612. [CrossRef]

87. Montoya, A.T.; Gillan, E.G. Photocatalytic Carbon Nitride Materials with Nanoscale Features Synthesized from the Rapid and Low-Temperature Decomposition of Trichloromelamine. *ACS Appl. Nano Mater.* **2018**, *1*, 5944–5956. [CrossRef]

88. Stagi, L.; Chiriu, D.; Ricci, P.C.; Corpino, R.; Ricci, P.C. Structural and optical properties of carbon nitride polymorphs. *Diam. Relat. Mater.* **2016**, *68*, 84–92. [CrossRef]

89. Porcu, S.; Roppolo, I.; Salaun, M.; Sarais, G.; Barbarossa, S.; Casula, M.F.; Carbonaro, C.M.; Ricci, P.C. Come to light: Detailed analysis of thermally treated Phenyl modified Carbon Nitride Polymorphs for bright phosphors in lighting applications. *Appl. Surf. Sci.* **2020**, *504*, 144330. [CrossRef]

90. Wang, Y.; He, J.; Chen, H.; Chen, J.; Zhu, R.; Ma, P.; Towers, A.; Lin, Y.; Gesquiere, A.J.; Wu, S.-T.; et al. Ultrastable, Highly Luminescent Organic-Inorganic Perovskite-Polymer Composite Films. *Adv. Mater.* **2016**, *28*, 10710–10717. [CrossRef] [PubMed]

91. Luridiana, A.; Pretta, G.; Chiriu, D.; Ricci, P.C.; Corpino, R.; Secci, F.; Frongia, A.; Stagi, L.; Ricci, P.C. A facile strategy for new organic white LED hybrid devices: Design, features and engineering. *RSC Adv.* **2016**, *6*, 22111–22120. [CrossRef]

92. Ricci, P.C.; Laidani, N.; Chiriu, D.; Salis, M.; Carbonaro, C.; Corpino, R. ALD growth of metal oxide on carbon nitride polymorphs. *Appl. Surf. Sci.* **2018**, *456*, 83–94. [CrossRef]

93. Qiao, Y.; Li, W.; Bao, J.; Zheng, Y.; Feng, L.; Ma, Y.; Yang, K.; Wu, A.; Bai, H.; Yang, Y. Controlled synthesis and luminescence properties of core-shell-shell structured SiO$_2$@AIPA-S-Si-Eu@SiO$_2$ and SiO$_2$@AIPA-S-Si-Eu-phen@SiO$_2$ nanocomposites. *Sci. Rep.* **2020**, *10*, 1–12. [CrossRef]

94. Sosa, J.D.; Bennett, T.F.; Nelms, K.; Liu, B.; Tovar, R.C.; Liu, Y. Metal–Organic Framework Hybrid Materials and Their Applications. *Crystals* **2018**, *8*, 325. [CrossRef]

95. Jang, S.; Song, S.; Lim, J.H.; Kim, H.S.; Phan, B.T.; Ha, K.-T.; Park, S.; Park, K.H. Application of Various Metal-Organic Frameworks (MOFs) as Catalysts for Air and Water Pollution Environmental Remediation. *Catalysis* **2020**, *10*, 195. [CrossRef]

96. Yu, X.; Wang, L.; Cohen, S. Photocatalytic metal–organic frameworks for organic transformations. *CrystEngComm* **2017**, *19*, 4126–4136. [CrossRef]

97. Mendiratta, S.; Lee, C.-H.; Lee, S.-Y.; Kao, Y.-C.; Chang, B.-C.; Lo, Y.-H.; Lu, K.-L. Structural Characteristics and Non-Linear Optical Behaviour of a 2-Hydroxynicotinate-Containing Zinc-Based Metal-Organic Framework. *Molcules* **2015**, *20*, 8941–8951. [CrossRef] [PubMed]

98. Zhan, X.-Q.; Yu, X.-Y.; Tsai, F.-C.; Ma, N.; Liu, H.-L.; Han, Y.; Xie, L.; Jiang, T.; Shi, D.; Xiong, Y. Magnetic MOF for AO7 Removal and Targeted Delivery. *Crystals* **2018**, *8*, 250. [CrossRef]

99. Cho, Y.J.; Yook, K.S.; Lee, J.Y. Cool and warm hybrid white organic light-emitting diode with blue delayed fluorescent emitter both as blue emitter and triplet host. *Sci. Rep.* **2015**, *5*, 7859. [CrossRef] [PubMed]

100. Mondal, T.; Mondal, S.; Bose, S.; Sengupta, D.; Ghorai, U.K.; Saha, S.K. Pure white light emission from a rare earth-free intrinsic metal–organic framework and its application in a WLED. *J. Mater. Chem. C* **2018**, *6*, 614–621. [CrossRef]

101. He, H.; Sun, F.; Borjigin, T.; Zhao, N.; Zhu, G. Tunable colors and white-light emission based on a microporous luminescent Zn(ii)-MOF. *Dalton Trans.* **2014**, *43*, 3716. [CrossRef]

102. Cui, Y.; Song, T.; Yu, J.; Yang, Y.; Wang, Z.; Qian, G. Dye Encapsulated Metal-Organic Framework for Warm-White LED with High Color-Rendering Index. *Adv. Funct. Mater.* **2015**, *25*, 4796–4802. [CrossRef]

103. Xuan, W.; Zhu, C.; Liu, Y.; Cui, Y. Mesoporous metal–organic framework materials. *Chem. Soc. Rev.* **2012**, *41*, 1677–1695. [CrossRef]

104. Sun, C.-Y.; Wang, X.-L.; Zhang, X.; Qin, C.; Li, P.; Su, Z.; Zhu, N.-X.; Shan, G.-G.; Shao, K.-Z.; Wu, H.; et al. Efficient and tunable white-light emission of metal–organic frameworks by iridium-complex encapsulation. *Nat. Commun.* **2013**, *4*, 2717. [CrossRef] [PubMed]